Radiology of colorectal cancer with emphasis on imaging of liver metastases

Pijl, M.E.J.

5

Quantitative Analysis of Focal Masses at MR Imaging: A Plea for Standardization

Milan E.J. Pijl, Joost Doornbos, Martin N.J.M. Wasser,
Hans C. van Houwelingen, Rob A.E.M. Tollenaar, Johan L. Bloem

Radiology 2004; 231: 737-744

ABSTRACT

Purpose: To assess the effects of changing analytic method variables on the signal intensity (SI) difference-to-noise ratios (SDNRs) for the contrast between lesions and background organs depicted on magnetic resonance (MR) images and to propose a standardized analytic method for the quantitative analysis of focal masses seen at MR imaging.

Materials and Methods: The SIs of 48 liver metastases (originating from colorectal cancer) in 20 patients, the surrounding liver parenchyma, and the background noise were measured on T2-weighted MR images. All 2000 and 2001 issues of the American Journal of Roentgenology, the Journal of Magnetic Resonance Imaging, Magnetic Resonance Imaging, and Radiology were searched for articles describing quantitative analyses. SDNRs were calculated by using formulas from these articles and various region of interest (ROI) locations to measure metastasis and background noise SIs. The Wilcoxon signed-rank test was used to compare the various SDNR calculations.

Results: In 34 articles in which quantitative analyses of focal masses are described, the reported SDNRs were calculated with four different formulas. The SDNRs for our study material calculated with the four formulas reported in the literature differed grossly in both number and unit. The SDNRs for ROIs encompassing the entire metastasis differed significantly ($P = .034$) from the SDNRs for ROIs in a homogeneous area of the metastasis margin. Differences in SDNRs between various noise ROI locations were significant ($P \leq .022$).

Conclusion: Slight changes in the variables of quantitative analysis of focal masses had marked effects on reported SDNRs. To overcome these effects, the use of a standardized method involving one formula, a lesion ROI in a homogeneous area at the metastasis margin, and a background noise ROI along the phase-encoding axis in the air (including systematic noise) is proposed for the quantitative analysis of findings on magnitude MR images.

INTRODUCTION

Quantitative analysis of focal masses visualized on magnetic resonance (MR) images is often used to optimize and compare MR imaging sequences and/or to characterize masses. Standardization of the analytic method and terminology used to determine the contrast generating properties of the images is crucial for the comparison of imaging study results. Many different methods for the quantitative analysis of focal masses have been described in the literature, however [1-7]. A variety of formulas have been used to calculate the contrast between lesions and background organs. The locations of the regions of interest (ROIs) used to measure the signal intensities (SIs) of background noise and lesions, if specified at all, vary among studies. Finally, with the exception of the preferred SI difference-to-noise ratio (SDNR) [8], different terms are used to express the contrast-generating properties of MR imaging sequences.

The purpose of this study was to assess the effects of changing analytic method variables on SDNRs for the contrast between lesions and background organs depicted on MR images and to propose a standardized analytic method for the quantitative analysis of focal masses seen at MR imaging.

MATERIALS AND METHODS

PATIENTS

For 14 months, a total of 33 consecutive patients who were either suspected of having or known to have colorectal cancer metastasis to the liver (i.e., colorectal liver metastasis) were referred to our hospital for partial liver resection or isolated liver perfusion with melphalan (Alkeran®; GlaxoSmithKline, Zeist, The Netherlands) [9] and were eligible for this study. The medical ethics committee of our hospital approved the protocol, and informed consent was obtained from all participating patients.

For 13 patients, there was no standard of reference because only hemangiomas were diagnosed (in one patient) or because of advanced disease (extrahepatic tumor or end-stage liver involvement in 12 patients). Thus, 20 patients (15 men, five women; mean age, 59 years; age range, 38-74 years) were included in this study. The mean age of both the women (age range, 38-72 years) and the men (age range, 45-74 years) was 59 years.

The primary malignancy was colorectal adenocarcinoma in all patients, each of whom

had at least one histologically proved metastasis to the liver. The diagnosis of liver metastases at the time of referral was established on the basis of an increased serum level of carcinoembryonic antigen in 11 patients and was supported by ultrasonographic (US) findings in eight and by computed tomographic (CT) findings in three patients. The diagnosis of liver metastasis was established on the basis of perioperative findings (synchronous liver metastases) at colorectal surgery in seven patients. In one patient each, the referral diagnosis was established with US only or CT only. In none of the patients was a relevant comorbidity of the liver, such as cirrhosis or steatosis, diagnosed. The median interval between preoperative MR imaging and surgery was 25 days (range, 3-124 days).

MR IMAGING

For this study, we used only a non-fat-suppressed respiratory-triggered T2-weighted fast spin-echo MR imaging sequence, which was performed with a 1.5-T system (Gyroscan NT 15; Philips Medical Systems, Best, The Netherlands) by using a quadrature body coil for signal transmission and reception. The effective echo time, echo spacing, and echo train length were 120 msec, 14 msec, and 16, respectively. Respiratory triggering was used, so the repetition time depended on the respiratory frequency (median repetition time, 2,100 msec; range, 1,750-2,500 msec). A belt placed around the upper abdomen generated the signal that was used for respiratory triggering.

The patients were not given special breathing instructions for the MR imaging examinations. Image acquisition was started just before end expiration, allowing data acquisition during a period of reduced respiratory motion. Eighteen 10 mm thick sections with a 1 mm intersection gap in the transverse orientation and anteroposterior phase-encoding direction were obtained with four acquired signals. The matrix size was 202 x 256. The field-of-view was 375 mm with a rectangular field-of-view of 80%; these parameters were balanced to achieve an optimal combination of spatial resolution and acquisition time and to generate a proper amount of air in the field-of-view to place the background noise ROI.

STANDARD OF REFERENCE

The standard of reference diagnosis for all patients was based on a combination of surgical, intra-operative ultrasound (IOUS), and histologic findings. After inspection of the entire

abdomen and complete mobilization of the liver, one of two surgeons (including R.A.E.M.T.) involved in the liver surgery palpated the liver bimanually. One of two available radiologists (M.E.J.P. or M.N.J.M.W., with 3 and 5 years of experience, respectively), with full knowledge of the preoperative data, performed IOUS by using an Aloka 2000 system (Aloka, Tokyo, Japan) with a 7.5-MHz transducer tailored for IOUS procedures.

We categorized lesions as malignant or benign on the basis of histologic findings, consistency at palpation, characteristic appearance, and compressibility at IOUS. Lesions were considered to be malignant if they were firm and uneven at palpation and had one or more of the following features at US [10]: irregular shape, irregular margin, bull's eye appearance, and/or amorphous calcifications. Lesions were considered to be benign if they were soft, compressible, and hyperechoic and had the geographic characteristics of a hemangioma or if they were firm, sharply defined, thin walled, anechoic and had the post-acoustic enhancement characteristics of a cyst. Lesions that did not meet these criteria were considered to be potentially malignant and were either resected or sampled at intra-operative fine-needle aspiration biopsy.

Thus, we identified 123 focal hepatic lesions: 95 were malignant, and 28 were benign (16 hemangiomas, 11 cysts, one granulomatous nodule). Twenty-one (22%) of the 95 metastases were confirmed at histologic analysis, and the remaining 74 (78%) were confirmed by using a combination of inspection, palpation, and IOUS findings. The median number of metastases per patient was four (range, 1-12). The location of each lesion was specified by using the Bismuth system [11].

The largest diameter of all metastases was assessed at IOUS. Thirty-four metastases were 10 mm in diameter or smaller, and 61 were larger than 10 mm in diameter. Their median diameter was 20 mm (range, 2-105 mm).

LITERATURE REVIEW

All issues of the American Journal of Roentgenology, the Journal of Magnetic Resonance Imaging, Magnetic Resonance Imaging, and Radiology published in 2000 and 2001 were searched article by article for studies in which SDNRs or contrast-to-noise ratios (CNRs) for focal lesions seen at MR imaging were reported.

The formulas used to calculate the SDNR or CNR and the size and location of ROIs in the lesions and background organs reported in each article were documented. In addition to

the size and location of the noise ROIs, the direction of the noise in relation to phase-encoding and the inclusion or exclusion of ghost artifacts were recorded. One author (M.E.J.P.) manually searched the journals, collected information on the quantitative analysis parameters, and subsequently calculated SDNRs for the liver metastases detected in the current series by using the formulas reported in these articles.

QUANTITATIVE ANALYSIS

One observer (M.E.J.P., with 3 years of experience) measured all SIs at a workstation (Easyvision; Philips Medical Systems) by using standard software (Philips Medical Systems) and operator-defined ROIs. All ROI measurements were performed on magnitude MR images. For each ROI, the mean SI and the standard deviation (SD) were determined.

All benign lesions were excluded from this analysis. To minimize the effects of partial volume averaging, only the 61 metastases with a diameter of greater than 10 mm were eligible for this analysis. Ten metastases that were identified by using the standard of reference could not be detected with MR imaging and therefore were not included in this quantitative analysis. Because of tumor compression of portal venous structures [12], a part of a right liver lobe that contained three metastases in one patient showed extensive edema. We excluded these three metastases from analysis because there was no normal liver parenchyma that could be used for reference. Thus, 48 metastases (median of two metastases per patient; range, 1-8 metastases), in 20 patients, larger than 10 mm in diameter were ultimately included in our quantitative analysis.

The SIs of the metastases were measured in two locations. For the first measurement, the ROI was placed in a homogeneous representative area at the margin of the metastasis, and for the second measurement, the ROI encompassed the entire metastasis. The median size of the first metastasis ROI was 21 mm^2 (range, 8-93 mm^2), and that of the second ROI was 560 mm^2 (range, 96-7,224 mm^2). An oval ROI was used to measure the SI at the margin of the metastasis, whereas the ROI covering the entire metastasis was identical to the shape of that particular metastasis.

The ROI in the liver parenchyma was located in the right lobe in an optically homogeneous area. Ghost artifacts and vessels were avoided as much as possible. In addition, the ROI in the liver parenchyma was oval and drawn as large as possible, but at least 1 cm^2.

The SI of the background noise was measured at four locations in the air outside the

patient, as illustrated in Figure 1: (a) in an oval area with the long axis along the phase-encoding direction, anterolateral to the right side of the abdomen; (b) in an oval area with the long axis perpendicular to the phase-encoding direction, in front of the right liver lobe; (c) in a rectangular area with the long axis perpendicular to the phase-encoding direction, in front of the entire liver; and (d) in a rectangular area with the long axis perpendicular to the phase-encoding direction, in front of the entire abdomen.

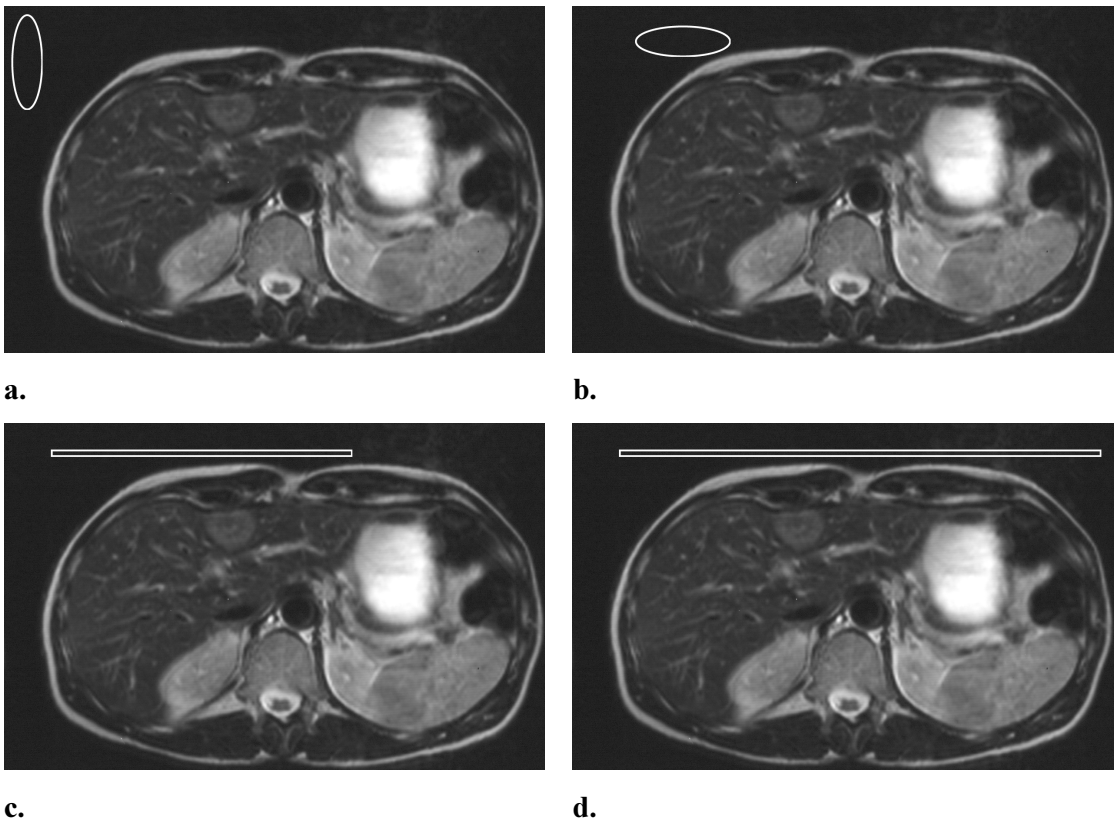

a. **b.**

c. **d.**

Figure 1. Transverse respiratory-triggered T2-weighted fast spin-echo MR images (120 msec effective echo time, 14 msec echo spacing, echo train length of 16) show background noise ROIs in the four locations relative to the liver and abdomen. (**a**) Oval ROI with long axis along the phase-encoding direction, anterolateral to the right side of the abdomen. (**b**) Oval ROI with long axis perpendicular to the phase-encoding direction, in front of the right liver lobe. (**c**) Rectangular ROI with long axis perpendicular to the phase-encoding direction, in front of the entire liver. (**d**) Rectangular ROI with long axis perpendicular to the phase-encoding direction, in front of the entire abdomen.

All background noise ROIs were drawn as large as possible; owing to field-of-view limitations, they were at least 4 cm^2. Ghost artifacts, if present, were not excluded from the noise ROIs. The choices of the locations described above were derived from the literature [1,4,13-18].

Since malignant tumors are often inhomogeneous, we applied a subjective optical ranking system. One observer (M.N.J.M.W.) who was neither involved in performing the ROI measurements nor aware of the measurement results ranked the extent of areas with low SI (fibrosis and/or calcification) and high SI (necrosis) in each metastasis. Areas of low and high SI were separately categorized by using a three-point scale: 0 meant no areas with high or low SI apparent; 1, small or punctate areas; and 2, large areas. For each metastasis, we combined the scores for these two categories (i.e., low- and high-SI areas) into a total optical score by subtracting the low-SI area score from the high-SI area score to classify metastasis inhomogeneity on a five-point scale: -2 indicated a metastasis with large areas of low SI; -1, a metastasis with some areas of low SI or with large areas of low SI and some areas of high SI; 0, a homogeneous metastasis or a metastasis with similar amounts of high- and low-SI areas; 1, a metastasis with some areas of high SI or with large areas of high SI and some areas of low SI; and 2, a metastasis with large areas of high SI.

To compare the formulas used to calculate the SDNR, we used fixed locations of metastasis and background noise ROIs: a homogeneous area at the margin of the metastasis and an oval noise ROI in front of the right liver lobe, respectively. We chose these ROI locations because we believed that they were the most appropriate.

STATISTICAL ANALYSES

The Wilcoxon signed-rank test was used to compare the various SDNR calculations. Since the formulas used to calculate the lesion-background organ SDNR that we found in the literature were quite different – both in scale and in unit – we believed that it was inappropriate to perform a statistical analysis of their ranking.

To quantify the relationships between the SDNRs calculated with the various formulas, the metastasis ROI locations, and the background noise ROI locations, Spearman correlation coefficients were used. All statistical comparisons were performed by using computer software (SPSS, version 10.0.5; SPSS, Chicago, Ill.). $P < .05$ was considered to indicate significance.

RESULTS

LITERATURE REVIEW

In 2000 and 2001, 34 articles in which focal lesion SDNRs or CNRs were reported were published in the American Journal of Roentgenology, the Journal of Magnetic Resonance Imaging, Magnetic Resonance Imaging, and Radiology. Twenty-three of these articles were focused on focal liver lesions [1,3-7,15-31]. The SDNRs or CNRs for focal lesions in the pancreas, female pelvis, kidney, and brain were reported, respectively, in two [2,32], two [33,34], two [35,36], and five [37-41] articles.

Four different formulas were used to calculate lesion-background organ SDNRs or CNRs in these 34 articles:

1. $(SI_L - SI_{BO}) / SD_N$ was used 26 times.
2. $(SI_L - SI_{BO}) / SI_N$ was used five times.
3. $(SI_L - SI_{BO}) / (SI_{BO} - SD_N)$ was used once.
4. $(SI_L - SI_{BO}) / (SI_{BM} - SD_N)$ was used once.
5. No formula was described in one article.

In these formulas, SI_L is the mean SI of the lesion; SI_{BO}, the mean SI of the background organ; SD_N, the SD of the background noise; SI_N, the mean SI of the background noise; and SI_{BM}, the mean SI of back muscles. The formula used to calculate the lesion-background organ SDNR was not described in one article [41].

The information about the ROIs in the focal lesions, background organs, and noise that is reported in the 34 articles is summarized in Table 1. Ghost artifacts were excluded from the noise ROI in six studies and were included in four. Only one article [1], similar to our report, included a description of all ROI data. In four (12%) of the 34 articles [6,23,32,38], detailed information about the ROIs was not provided.

QUANTITATIVE ANALYSIS

The SI measurements in the 48 colorectal liver metastases in the 20 patients in the present study are summarized in Table 2. The SDNRs for these metastases, as calculated by using the four formulas reported in the literature, are presented in Table 3.

Table 1. ROI Information Reported.

ROI Data Reported	No. of Articles (n = 34)
Lesion	
Location	11 (32)
Size	19 (56)
Background organ	
Location	15 (44)
Size	7 (21)
Background noise	
Location	25 (74)
Size	5 (15)
Direction as related to phase-encoding	19 (56)
Inclusion or exclusion of ghost artifacts	10 (29)

Numbers in parentheses are percentages.

Table 2. SI Measurements for ROI Locations in 48 Liver Metastases.

ROI[#]	SI[†]
Metastases	
Lesion margin	590 ± 21
Entire lesion	568 ± 94
Liver parenchyma	321 ± 33
Background noise	
Right anterolateral area	21 ± 12
In front of right liver lobe	45 ± 26
In front of liver	47 ± 30
In front of abdomen	61 ± 44

[#] ROI locations are described in the Quantitative Analysis section of the Materials and Methods.
[†] Data are mean SIs ± SDs.

Although the direct comparison of SDNR values was not appropriate, as stated before, the magnitude of numeric differences in the SDNR values calculated with the four formulas was striking. For any of the 48 metastases, the purely numeric SDNR was largest when it was calculated with formula 1, and it always decreased in the same order, via formulas 2 and 3, to

the smallest SDNR calculated with formula 4. The SDNRs calculated with formulas 1 and 2 showed excellent correlation (Spearman $\rho = 0.97$), as demonstrated in Figure 2. On average, the SDNR calculated with formula 1 was 1.78 times the SDNR calculated with formula 2.

Table 3. Mean SDNRs for 48 Liver Metastases Calculated with Four Different Formulas.

Formula No.	Formula[#]	SDNR[†]
1	$(SI_L - SI_{BO}) / SD_N$	11.5 ± 5.7
2	$(SI_L - SI_{BO}) / SI_N$	6.4 ± 3.0
3	$(SI_L - SI_{BO}) / (SI_{BO} - SD_N)$	1.0 ± 0.5
4	$(SI_L - SI_{BO}) / (SI_{BM} \times SD_N)$	0.05 ± 0.03

[#] SI_L is the mean SI of the lesion; SI_{BO} the mean SI of the background organ; SD_N the SD of the background noise; SI_N the mean SI of the background noise; and SI_{BM} the mean SI of back muscles.
[†] Mean SDNRs ± SDs.

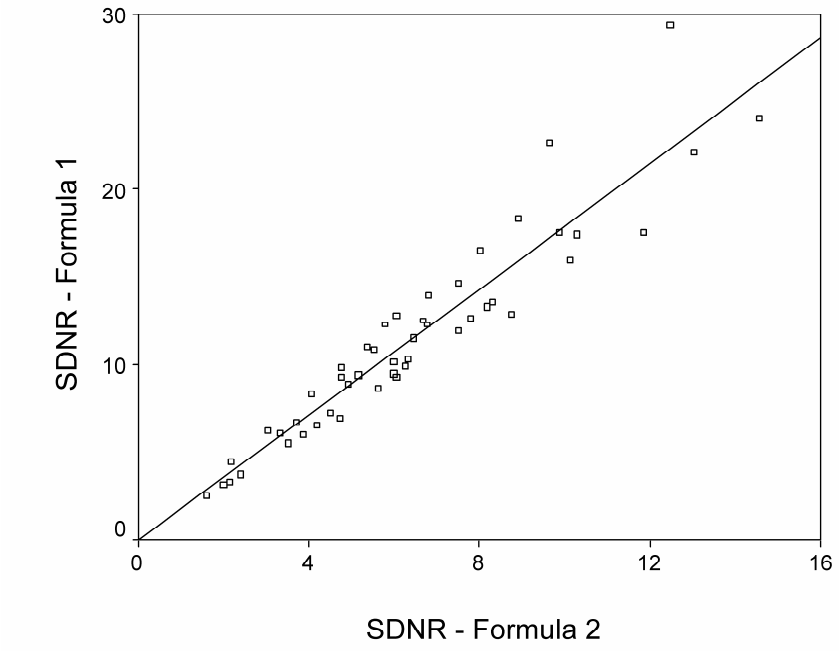

Figure 2. Scatterplot of SDNRs calculated with formula 1, $(SI_L - SI_{BO}) / SD_N$, and formula 2, $(SI_L - SI_{BO}) / SI_N$, shows the scale of SDNRs and the high correlation (Spearman $\rho = 0.97$) between values calculated with the two formulas. The scatterplot data indicate the possibility of converting formula 1 to formula 2 and vice versa. Note that the agreement between the two sets of values is very good in the lower regions and poorer in the higher regions.

The correlation coefficients for the relationship between SDNRs calculated with formulas 1 and 2 and SDNRs calculated with formulas 3 and 4 ranged from 0.60 to 0.75. The correlation coefficient for the relationship between SDNRs calculated with formulas 3 and 4 was 0.48.

The SDNRs for the two ROI locations in the metastasis (i.e., at the margin or encompassing the entire lesion) were calculated with formula 2. We preferred formula 2 over formula 1 because the SDNRs were calculated from magnitude MR images in this clinical setting [13]. For the 48 colorectal liver metastases, the mean SDNRs for the ROIs at the margin and for those encompassing the entire lesion were 6.4 ± 3.0 (SD) and 6.0 ± 3.5, respectively. The SDNR for the marginal ROI was larger than, smaller than, or equal to that for the ROI encompassing the entire metastasis in 31 metastases, 16 metastases, and one metastasis (P = .034), respectively, indicating metastasis inhomogeneity. The Spearman ρ was 0.89 for the correlation between margin ROI and entire-lesion ROI SDNR values.

Table 4. SDNRs for ROIs Placed in Metastases.

Total Optical Score and ROI	SDNR[#]	Positive Rank[†]	Negative Rank[†]	Tie in Rank[†]
-2				
Lesion margin	4.0 ± 1.5	6	0	0
Entire lesion	2.4 ± 0.5			
-1				
Lesion margin	6.3 ± 2.3	17	2	0
Entire lesion	5.1 ± 1.9			
0				
Lesion margin	6.4 ± 3.5	8	5	1
Entire lesion	6.6 ± 3.9			
+1				
Lesion margin	8.2 ± 3.5	0	9	0
Entire lesion	9.3 ± 3.8			

[#] Mean SDNRs ± SDs. All SDNRs were calculated with formula number 2: $(SI_L - SI_{BO}) / SI_N$, where SI_L is the mean SI of the lesion; SI_{BO} the mean SI of the background organ; and SI_N the mean SI of the background noise.

[†] Data are numbers of metastases. Positive rank indicates that the SDNR for the ROI at the margin of the metastasis was larger than the SDNR for the ROI encompassing the entire metastatic lesion. Negative rank indicates that the margin SDNR was smaller than the entire SDNR. Tie in rank indicates that the margin and entire SDNRs were equal.

The total optical scores calculated for the presence of high- and low-SI areas were -2 for six, -1 for 19, 0 for 14, 1 for nine, and 2 for zero metastases. The mean SDNRs and total optical scores for the ROIs at the metastasis margins and for those encompassing the entire metastases are reported in Table 4. The presented rank data indicate significant differences in SDNRs between the "margin" and "entire" metastasis ROIs with calculated optical scores of -2, -1, and 1, with *P* values of .028, less than .001, and .008, respectively. We observed no significant difference (*P* = .92) in SDNRs between the two ROI groups among those with a calculated optical score of 0. Spearman ρ values were 0.43, 0.93, 0.93, and 0.97 for the metastasis ROIs with calculated optical scores of -2, -1, 0, and 1, respectively.

To calculate metastasis-liver parenchyma SDNRs for the various noise ROI locations, we used the same formula (formula 2) and a ROI in a homogeneous representative area at the margin of the metastasis. The SDNRs and surface areas of background noise ROIs in the four locations are presented in Table 5. The differences in SDNR among the various noise ROI locations were highly significant. The SDNR for the noise ROI anterolateral to the abdomen was always higher than those for the ROIs in the other locations (*P* < .001). The SDNR for the oval noise ROI in front of the right liver lobe was always higher than that for the rectangular noise ROI in front of the entire abdomen (*P* < .001). The SDNR for the oval noise ROI in front of the right liver lobe was larger than, smaller than, or equal to that for the rectangular noise ROI in front of the entire liver in 25, 16, and seven metastases, respectively (*P* = .022). The SDNR for the rectangular noise ROI in front of the entire abdomen was larger than, smaller than, or equal to the SDNR for the rectangular noise ROI in front of the entire liver in three, 45, and zero metastases, respectively (*P* < .001).

Table 5. SDNRs and Surface Areas for Background Noise ROI Locations in 20 Patients.

Location of Background Noise ROI	Metastasis-Liver SDNR[#]	Mean Surface Area of ROI[†]
Right anterolateral area	13.8 ± 7.1	1,159
In front of right liver lobe	6.4 ± 3.0	1,142
In front of liver	6.2 ± 3.1	800
In front of abdomen	4.7 ± 2.4	1,575

[#] Mean SDNRs ± SDs. All SDNRs were calculated with formula number 2: $(SI_L - SI_{BO}) / SI_N$, where SI_L is the mean SI of the lesion; SI_{BO} the mean SI of the background organ; and SI_N the mean SI of the background noise.

[†] Data are ROI surface areas in mm^2.

The SDNRs for the several noise ROIs correlated well. Spearman ρ values ranged from the largest value of 0.98 for the correlation between the SDNR for the oval noise ROI in front of the right liver lobe and the SDNR for the rectangular noise ROI in front of the entire liver (Figure 3) to the smallest value of 0.92 for the correlation between the SDNR for the oval noise ROI anterolateral to the abdomen and the SDNR for the rectangular noise ROI in front of the entire abdomen.

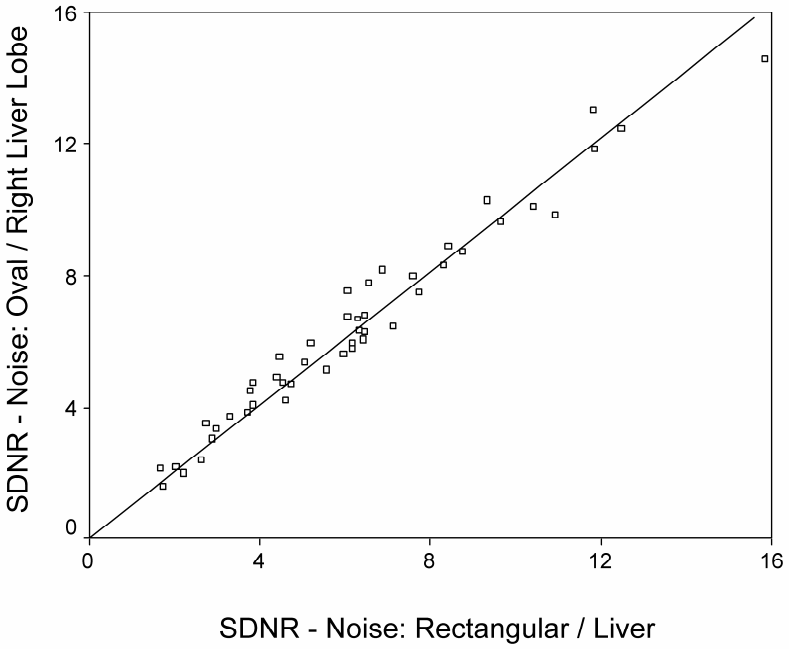

Figure 3. Scatterplot of SDNRs for oval background noise ROIs with the long axis perpendicular to the phase-encoding direction, in front of the right liver lobe versus SDNRs for rectangular ROIs with the long axis perpendicular to the phase-encoding direction, in front of the entire liver. The scatterplot data indicate the absence of a systematic difference in SDNRs between the two ROIs (i.e., equal scales) and a high correlation between the two sets of values (Spearman $\rho = 0.98$).

DISCUSSION

Many methods can be used for the quantitative analysis of focal masses depicted on MR images, but apparently slight changes in the method can result in important numeric changes in calculated metastasis-liver parenchyma SDNRs, as demonstrated in our series. SDNR should be the preferred term used to express image quality in daily practice [8] since CNR is display-dependent (i.e., is based on digital pixel values and window width and level).

In the literature search that we performed, the information concerning the quantitative analysis parameters, the locations of the ROIs, and the formulas used to calculate the lesion-

background organ SDNR was often incomplete. The various formulas used to calculate lesion-background organ SDNRs that we found in the literature were not equal in unit and had numeric differences over a factor of 200 when we used them for our study material. The metastasis-liver parenchyma SDNRs for the various locations of metastasis (P = .034) and background noise (maximal P = .022) ROIs were significantly different.

Not surprisingly, the metastasis-liver parenchyma SDNR was larger when the formula in which the background noise SD was the denominator (formula 1) was used, as compared with the SDNR calculated with the background noise SI as the denominator (formula 2), because the background noise SI is always the larger number. The SDNRs calculated with formulas 3 and 4 differed substantially from those calculated with formulas 1 and 2 – not only in numeric value but also in unit – and thus in our opinion should not be compared with data calculated with formulas 1 and 2. Furthermore, no theoretic background information can be obtained for the rarely used formulas 3 and 4 [8,13,14].

The choice of whether to use formula 1 or formula 2 is more difficult, although formula 2, as explained by Kaufman et al [13], seems the preferable one when SDNRs are calculated from magnitude MR images. However, this choice might be less important because a ratio of the average noise level to the SD of the average noise level exists on magnitude MR images [42]. Henkelman [42] reported a theoretic average noise level-to-SD of average noise level ratio of 1.91 and a tested ratio of 1.92 in areas without motion artifacts. In our study, with the presence of motion artifacts, this ratio was 1.78. The strong mathematic relationship between SDNRs calculated with formulas 1 and 2 is reflected by the high correlation coefficient (Spearman ρ = 0.97) obtained when we compared the results obtained with these two formulas. If real rather than magnitude MR images are used, with a resulting background noise SI of around 0, then the noise data must be manipulated, and, consequently, the SD of the manipulated background noise SI should be used, as explained by Kaufman et al [13].

As far as we know, no theoretic background information on the placement of lesion ROIs has been reported. It seems common sense to place the ROI in viable tumor tissue and to avoid areas of the lesion with extreme SI, both high and low. When these areas with high or low SI are large enough relative to the lesion size, they might make the lesion more conspicuous, but they artificially increase or decrease the calculated SDNR. Thus, we think that the margin of a neoplasm, which is virtually always the viable growing part of the lesion, is the region that truly generates contrast with the surrounding tissue. This seems especially

important when homogeneous or small lesions, which typically lack areas with extreme SI values, are considered because the viable peripheral component of neoplasms is likely to exhibit the same SI characteristics as that of homogeneous or small lesions consisting entirely of viable tumor.

Our study results demonstrate that significant (P = .034) differences in SDNRs were seen when the ROI at the margin of the metastasis was compared with the ROI encompassing the entire metastasis. When the SDNRs were stratified according to lesion inhomogeneity by using a qualitative factor – specifically, the total optical score – these differences increased for inhomogeneous lesions ($P \leq .028$) but almost disappeared for both lesions containing equal amounts of high- and low-SI areas and homogeneous lesions (P = .92).

In general, noise in an image can obliterate diagnostic information and consists of statistical and systematic components [14]. Statistical noise spreads almost evenly over an image, whereas systematic noise, depending on its source, can be structured or have some sort of distribution pattern. In general, as stated by Kaufman et al [13], noise should be measured in the air outside of the object being imaged, along the frequency-encoding axis, and away from the filter cutoff region. In the Kaufman et al article, the authors report that for comparison purposes, if one is interested in overall image quality, noise can also be measured along the phase-encoding axis. However, the trade-off for measuring noise in this direction is that the existence of systematic noise, such as that generated by patient motion – for example, breathing – may lead to an overestimation of noise and subsequently a decrease in the SDNR.

Because good overall image quality is crucial for focal lesion detection, we believe that in studies of focal lesion detection, noise should be measured along the phase-encoding axis. Second, since ghost artifacts clearly influence overall image quality, they should not be avoided when placing noise ROIs. Therefore, the noise ROI should not be placed anterolateral to the right side of the abdomen because in this location, systematic noise is almost completely avoided, and, thus, the SDNR will be artificially elevated. Also, the noise ROI should not be placed in front of the entire abdomen because noise generated to the left of the liver will be included in the ROI, and this will cause the SDNR to be artificially decreased.

The choice of whether to place an oval noise ROI in front of the right liver lobe or a rectangular noise ROI in front of the entire liver is less obvious and, in view of the high correlation (Spearman $\rho = 0.98$) of SDNRs measured in these two areas, less important. In the end, we preferred the oval ROI in front of the right liver lobe rather than the rectangular ROI

for measuring noise because the oval region has a larger diameter in the phase-encoding direction, and, thus, selecting it will ensure the inclusion of ghost artifacts generated from breathing, if they are present. Second, the geometry of an oval ROI allows a larger surface area than does that of a rectangular ROI because of the geometry of air within the field-of-view. In general, if one wants to perform a quantitative analysis, both the field-of-view and the rectangular field-of-view should be chosen in a manner such that enough space (i.e., air) is available for the correct placement of the background noise ROI.

Although our goal was to demonstrate the effects of changing variables in the analytic method itself, and we believe that this goal is minimally influenced by the MR imaging technique used, a few limitations apply to the MR imaging technique that we used. First, a single pulse sequence was performed by using a machine from only one vendor. Second, the MR images were acquired by using a body coil instead of a phased-array coil, and this resulted in smaller SDNRs. The use of a phased-array coil, though, requires paying extra attention to the placement of the background noise ROI owing to the less uniform SI profile of this coil. To minimize these effects, when a phased-array coil is used, one should describe its exact position and measure the background noise at a fixed distance from the coil. Third, the use of a 10 mm section thickness and the exclusion of metastases 10 mm or smaller left the possibility of partial volume effects. When drawing the ROIs, we paid special attention not to include any normal tissue by keeping a safe distance from the lesion border; however, complete avoidance of tissue averaging can never be guaranteed. Fourth, since for some patients more than one metastasis was included in the analysis, SI interdependence could not be excluded and might have influenced outcomes. Finally, since the anteroposterior diameter of the rectangular noise ROI in front of the entire liver is relatively small compared with the diameter of the oval noise ROI in front of the right liver lobe, there is the chance that ghost artifacts will be missed and consequently that the SDNR will be overestimated.

Since apparently slight changes in the analytic method can result in important numeric changes in calculated metastasis-liver parenchyma SDNRs, we propose the use of a standardized method for the quantitative analysis of focal masses depicted on MR images that includes an accurate description of the ROIs. In our opinion, the SDNR on magnitude MR images should be calculated by using the formula $(SI_L - SI_{BO}) / SI_N$, where SI_L is the mean SI of the lesion; SI_{BO}, the mean SI of the background organ; and SI_N, the mean SI of the background noise. The lesion ROI should be placed in a homogeneous representative area at

the margin of the lesion, and the background noise ROI should be placed along the phase-encoding axis in the air and include systematic noise, such as that generated from motion artifacts, since they influence overall image quality. In addition, the background organ ROI must be in a homogeneous representative part of the organ.

REFERENCES

1. Paley MR, Mergo PJ, Torres GM, Ros PR. Characterization of focal hepatic lesions with ferumoxides-enhanced T2-weighted MR imaging. AJR Am J Roentgenol 2000; 175:159-163.
2. Thoeni RF, Mueller-Lisse UG, Chan R, Do NK, Shyn PB. Detection of small, functional islet cell tumors in the pancreas: selection of MR imaging sequences for optimal sensitivity. Radiology 2000; 214:483-490.
3. Ward J, Guthrie JA, Scott DJ, et al. Hepatocellular carcinoma in the cirrhotic liver: double-contrast MR imaging for diagnosis. Radiology 2000; 216:154-162.
4. Scott J, Ward J, Guthrie JA, Wilson D, Robinson PJ. MRI of liver: a comparison of CNR enhancement using high dose and low dose ferumoxide infusion in patients with colorectal liver metastases. Magn Reson Imaging 2000; 18:297-303.
5. Ba-Ssalamah A, Heinz-Peer G, Schima W, et al. Detection of focal hepatic lesions: comparison of unenhanced and SHU 555 A-enhanced MR imaging versus biphasic helical CTAP. J Magn Reson Imaging 2000; 11:665-672.
6. Aschoff AJ, Merkle EM, Wong V, et al. How does alteration of hepatic blood flow affect liver perfusion and radiofrequency-induced thermal lesion size in rabbit liver? J Magn Reson Imaging 2001; 13:57-63.
7. Braga HJV, Imam K, Bluemke DA. MR imaging of intrahepatic cholangiocarcinoma: use of ferumoxides for lesion localization and extension. AJR Am J Roentgenol 2001; 177:111-114.
8. Wolff SD, Balaban RS. Assessing contrast on MR images. Radiology 1997; 202:25-29.
9. Rothbarth J, Pijl ME, Vahrmeijer AL, et al. Isolated hepatic perfusion with high-dose melphalan for the treatment of colorectal metastasis confined to the liver. Br J Surg 2003; 90:1391-1397.
10. Cosgrove DO. Malignant liver disease. In: Meire HB, Cosgrove DO, Dewbury KC, Farrant P, eds. Abdominal and general ultrasound. 2nd ed. London: Churchill Livingstone, 2001; 209-234.
11. Bismuth H. Surgical anatomy and anatomical surgery of the liver. World J Surg 1982; 6:3-9.
12. Itai Y, Ohtomo K, Furui S, Minami M, Yoshikawa K, Yashiro N. Lobar intensity differences of the liver on MR imaging. J Comput Assist Tomogr 1986; 10:236-241.

13. Kaufman L, Kramer DM, Crooks LE, Ortendahl DA. Measuring signal-to-noise ratios in MR imaging. Radiology 1989; 173:265-267.
14. Hendrick RE. Measurement of signal, noise, and SNR in MR Images. In: Hendrick RE, Russ PD, Simon JH, eds. MRI: principles and artifacts. 1st ed. New York: Raven Press Ltd., 1993; 2-6.
15. Mori K, Yoshioka H, Itai Y, et al. Arterioportal shunts in cirrhotic patients: evaluation of the difference between tumorous and nontumorous arterioportal shunts on MR imaging with superparamagnetic iron oxide. AJR Am J Roentgenol 2000; 175:1659-1664.
16. Runge VM, Kenney CM. Phase II double-blind, dose-ranging clinical evaluation of gadobenate dimeglumine in focal liver lesions: with analysis of liver and kidney signal change on early and delayed imaging. J Magn Reson Imaging 2000; 11:655-664.
17. Aschoff AJ, Rafie N, Jesberger JA, Duerk JL, Lewin JS. Thermal lesion conspicuity following interstitial radiofrequency thermal tumor ablation in humans: a comparison of STIR, turbo spin-echo T2-weighted, and contrast-enhanced T1-weighted MR images at 0.2 T. J Magn Reson Imaging 2000; 12:584-589.
18. Jeong YY, Mitchell DG, Holland GA. Liver lesion conspicuity: T2-weighted breath-hold fast spin-echo MR imaging before and after gadolinium enhancement - initial experience. Radiology 2001; 219:455-460.
19. Materne R, Horsmans Y, Jamart J, Smith AM, Gigot JF, Van Beers BE. Gadolinium-enhanced arterial-phase MR imaging of hypervascular liver tumors: comparison between tailored and fixed scanning delays in the same patients. J Magn Reson Imaging 2000; 11:244-249.
20. Nakayama M, Yamashita Y, Mitsuzaki K, et al. Improved tissue characterization of focal liver lesions with ferumoxide-enhanced T1 and T2-weighted MR imaging. J Magn Reson Imaging 2000; 11:647-654.
21. Matsuo M, Kanematsu M, Murakami T, et al. T2-weighted MR imaging for focal hepatic lesion detection: supplementary value of breath-hold imaging with half-Fourier single-shot fast spin-echo and multishot spin-echo echoplanar sequences. J Magn Reson Imaging 2000; 12:444-452.
22. Kanematsu M, Itoh K, Matsuo M, et al. Malignant hepatic tumor detection with ferumoxides-enhanced MR imaging with a 1.5-T system: comparison of four imaging pulse sequences. J Magn Reson Imaging 2001; 13:249-257.
23. Pauleit D, Textor J, Bachmann R, et al. Improving the detectability of focal liver lesions on T2-weighted MR images: ultrafast breath-hold or respiratory-triggered thin-section MRI? J Magn Reson Imaging 2001; 14:128-133.

24. Katayama M, Masui T, Kobayashi S, et al. Fat-suppressed T2-weighted MRI of the liver: comparison of respiratory-triggered fast spin-echo, breath-hold single-shot fast spin-echo, and breath-hold fast-recovery fast spin-echo sequences. J Magn Reson Imaging 2001; 14:439-449.
25. Hori M, Murakami T, Kim T, et al. Single breath-hold T2-weighted MR imaging of the liver: value of single-shot fast spin-echo and multishot spin-echo echoplanar imaging. AJR Am J Roentgenol 2000; 174:1423-1431.
26. Raman SS, Lu DS, Chen SC, Sayre J, Eilber F, Economou J. Hepatic MR imaging using ferumoxides: prospective evaluation with surgical and intraoperative sonographic confirmation in 25 cases. AJR Am J Roentgenol 2001; 177:807-812.
27. Lim JH, Choi D, Cho SK, et al. Conspicuity of hepatocellular nodular lesions in cirrhotic livers at ferumoxides-enhanced MR imaging: importance of Kupffer cell number. Radiology 2001; 220:669-676.
28. Rydberg JN, Tervonen OA, Rydberg DB, Lomas DJ, Ehman RL, Riederer SJ. Dual-echo breathhold T(2)-weighted fast spin echo MR imaging of liver lesions. Magn Reson Imaging 2000; 18:117-124.
29. Pawluk RS, Borrello JA, Brown JJ, McFarland EG, Mirowitz SA, Tsao LY. A prospective assessment of breath-hold fast spin echo and inversion recovery fast spin echo techniques for detection and characterization of focal hepatic lesions. Magn Reson Imaging 2000; 18:543-551.
30. Papanikolaou N, Moulopoulos LA, Gouliamos A, Ispanopoulou S, Vlahos L. Comparison of dual spin echo echo planar imaging (SE-EPI), turbo spin echo with fat suppression and conventional dual spin echo sequences for T(2)-weighted MR imaging of focal liver lesions. Magn Reson Imaging 2000; 18:715-719.
31. Yoshioka H, Itai Y, Saida Y, Mori K, Mori H, Okumura T. Superparamagnetic iron oxide-enhanced MR imaging for early and late radiation-induced hepatic injuries. Magn Reson Imaging 2000; 18:1079-1088.
32. Romijn MG, Stoker J, van Eijck CH, van Muiswinkel JM, Torres CG, Lameris JS. MRI with mangafodipir trisodium in the detection and staging of pancreatic cancer. J Magn Reson Imaging 2000; 12:261-268.
33. Masui T, Katayama M, Kobayashi S, Sakahara H, Ito T, Nozaki A. T2-weighted MRI of the female pelvis: comparison of breath-hold fast-recovery fast spin-echo and nonbreath-hold fast spin-echo sequences. J Magn Reson Imaging 2001; 13:930-937.
34. Seki H, Takano T, Sakai K. Value of dynamic MR imaging in assessing endometrial carcinoma involvement of the cervix. AJR Am J Roentgenol 2000; 175:171-176.

35. Scialpi M, Di Maggio A, Midiri M, Loperfido A, Angelelli G, Rotondo A. Small renal masses: assessment of lesion characterization and vascularity on dynamic contrast-enhanced MR imaging with fat suppression. AJR Am J Roentgenol 2000; 175:751-757.
36. Aschoff AJ, Sulman A, Martinez M, et al. Perfusion-modulated MR imaging-guided radiofrequency ablation of the kidney in a porcine model. AJR Am J Roentgenol 2001; 177:151-158.
37. Essig M, Deimling M, Hawighorst H, Debus J, van Kaick G. Assessment of cerebral gliomas by a new dark fluid sequence, High Intensity REduction (HIRE): a preliminary study. J Magn Reson Imaging 2000; 11:506-517.
38. Patola WB, Coulter BA, Chipperfield PM, Lingawi SS. A comparison of conventional spin-echo and fast spin-echo in the detection of multiple sclerosis. J Magn Reson Imaging 2001; 13:657-667.
39. Ba-Ssalamah A, Schick S, Herneth AM, et al. Preoperative fast MRI of brain tumors using three-dimensional segmented echo planar imaging compared to three-dimensional gradient echo technique. Magn Reson Imaging 2000; 18:635-640.
40. Ba-Ssalamah A, Schick S, Heimberger K, et al. Ultrafast magnetic resonance imaging of the brain. Magn Reson Imaging 2000; 18:237-243.
41. Essig M, Schoenberg SO, Debus J, van Kaick G. Disappearance of tumor contrast on contrast-enhanced FLAIR imaging of cerebral gliomas. Magn Reson Imaging 2000; 18:513-518.
42. Henkelman RM. Measurement of signal intensities in the presence of noise in MR images. Med Phys 1985; 12:232-233.